SCIENTIFIC REPORTS

OPEN

SUBJECT AREAS:
FLUIDS
ELECTRONIC MATERIALS AND DEVICES
APPLIED PHYSICS
MATERIALS PHYSICS

Received
23 September 2011

Accepted
23 November 2011

Published
7 December 2011

Correspondence and requests for materials should be addressed to S.A. (steve.arscott@iemn.univ-lille1.fr)

Moving liquids with light: Photoelectrowetting on semiconductors

Steve Arscott

Institut d'Electronique, de Microélectronique et de Nanotechnologie (IEMN), CNRS UMR8520, The University of Lille, Cité Scientifique, Avenue Poincaré, 59652 Villeneuve d'Ascq, France.

By linking semiconductor physics and wetting phenomena a brand new effect termed "photoelectrowetting-on-semiconductors" is demonstrated here for a conducting droplet resting on an insulator-semiconductor stack. Optical generation of carriers in the space-charge region of the underlying semiconductor alters the capacitance of the liquid-insulator-semiconductor stack; the result of this is a modification of the wetting contact angle of the droplet upon illumination using above band gap light. The effect is demonstrated using commercial silicon wafers, both n- and p-type having a doping range spanning four orders of magnitude ($6\times10^{14}-8\times10^{18}$ cm^{-3}), coated with a commercial amorphous fluoropolymer insulating film (Teflon®). Impedance measurements confirm that the observations are semiconductor space-charge related effects. The impact of the work could lead to new silicon-based technologies in areas such as Laboratory-on-a-Chip, Microfluidics and Optofluidics.

Liquid transport in microchip-based systems[1–7] is important in many areas such as Laboratory-on-a-chip[8], Microfluidics[9] and Optofluidics[10]. Actuation of liquids in such systems is usually achieved using either mechanical displacement[11] e.g. pumping or via energy conversion e.g. electrowetting[12–15] which modifies wetting. However, at the moment there is no clear way of actuating a liquid using light. The advantage of light actuation is clear: it would eliminate the need for pumps[11] and complex electronic circuitry currently used for droplet transport[12–15]. Here, a brand new effect "photoelectrowetting on semiconductors" (PWOS) is demonstrated and explained by linking semiconductor physics[16] and wetting phenomena[17].

Over a hundred years after pioneering work on electro-capillarity phenomena[18], electrowetting has undergone a recent renaissance via the use of microtechnology[12–15]. Briefly, when a droplet of conducting liquid, e.g. an electrolyte, is placed on a conductor coated with a thin layer of insulating material (Figure 1) the wetting contact angle θ of the droplet can be modified by applying a voltage V according to the Young-Lippmann equation[17]:

$$\cos\theta = \cos\theta_0 + C\frac{V^2}{2\gamma}$$

where θ_0 is the wetting contact angle at zero bias, C is the capacitance (per unit surface) of the insulating layer and γ is the surface tension of the liquid droplet. Note that C *does not vary* with either applied voltage or illumination for the liquid-insulator-conductor (LIC) system and the effect is *symmetrical with voltage polarity*, i.e. $\theta_{-V} = \theta_{+V}$. The effect has led to applications[13] such as displays[19,20], microelectromechanical systems[21], tunable optics[22] and digital-microfluidics[23,24] but still holds fundamental scientific challenges[15].

In contrast, if we now replace the conductor in Figure 1 by a *semiconductor* to form a liquid-insulator-semiconductor (LIS) stack shown in Figure 2a, space-charge effects in the semiconductor can now modify the electrowetting behaviour as C can change with both applied voltage[16] *and* illumination[25]. The reason for this is that C is now composed of two capacitances connected in series: C_i, the insulator capacitance and C_s the *voltage and illumination dependent capacitance* of the space-charge region in the semiconductor (Figure 2b); an effect much exploited for image sensing[26,27].

By borrowing well-known language from semiconductor physics[16] we should be able to make some simple predictions about the electrowetting behaviour of the LIS system by making the analogy with the well-known metal-insulator-semiconductor (MIS) system. Indeed it is well known that depletion layers form at electrolyte-semiconductor interfaces[28,29]; this effect has been exploited for commercial purposes[30,31] and electrolyte-semiconductor[32] and electrolyte-insulator-semiconductor[33] interfaces have been used for transistor-based sensing[34,35] and carbon nanotube transistors[36].

Straight away one can predict major differences compared to the LIC system: the electrowetting behaviour (i) will be *asymmetrical* with voltage polarity ($\theta_{-V} \neq \theta_{+V}$) (ii) will depend on the doping *density* and *type* of the

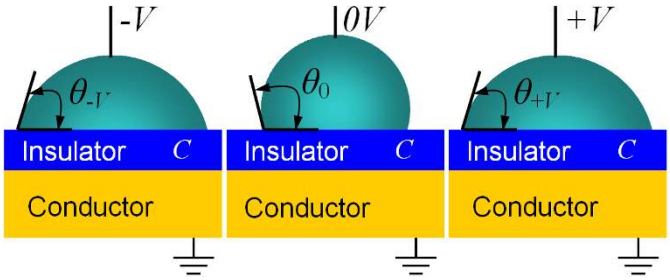

Figure 1 | Electrowetting behaviour for the liquid-insulator-conductor system. The variation of the contact angle of the droplet is symmetrical with the applied voltage polarity, $\theta_{-V} = \theta_{+V}$, and obeys the Young-Lippmann equation. The capacitance of the insulating layer is C Fm^{-2}; the conductor is considered to be perfect; the liquid is considered to be conducting.

underlying semiconductor and (iii) will depend on *illumination* (the value of C_s, can be modified by incident above band gap radiation)[16,25], (iv) under accumulation or high doping density should behave as the regular LIC system and (v) will be governed by other semiconductor effects, e.g. carrier inversion and breakdown[16] at higher bias.

Figure 2c shows the predicted effect of illumination using above band gap light on a biased LIS system in *depletion*. Light penetrating into the semiconductor will generate electron-hole pairs in the depletion zone[16]; the effect of this is to *increase* the capacitance of the stack[25] and thus *reduce* the contact angle of the droplet *at constant applied voltage*, i.e. the droplet spreads out upon illumination. Provided that there is no electrochemistry during illumination, e.g. due to breakdown of the insulator or the semiconductor, then the effect should be reversible.

The simple arguments above are based on the following assumptions: (i) the Debye length λ_D in the electrolyte (see Supplementary Information) is much less than the thickness of the insulator and the depletion width in the semiconductor meaning electrical double layer (EDL) effects[32,33] need not be considered, (ii) the capacitance is uniform under the droplet[37] and (iii) interface effects are ignored for the moment (surface states, trapped charge, mobile ionic charge in the insulator, high field effects…)[16].

Results

In order to test the above ideas commercial 3″ silicon wafers (Siltronix, France) were coated with an amorphous fluoropolymer layer of polytetrafluoroethylene (PTFE). PTFE is commercially available as Teflon® AF (Dupont, USA). Fluoropolymer films are currently being investigated for transistor gate dielectric[38,39]. The Teflon® thicknesses were 265 nm (±15 nm) and 20 nm (±3 nm) using spin coating (see Supplementary Information). Near field microscopy (tapping mode Atomic Force Microscopy) revealed that the Teflon® films were very smooth (roughness $R_q < 1$ nm) and defect free (see Supplementary Information). Four types of silicon wafers were employed: p-type ($N_A \sim 1.8\times10^{15}$ cm^{-3} and $N_A \sim 8\times10^{18}$ cm^{-3}) and n-type ($N_D \sim 6\times10^{14}$ cm^{-3} and $N_D \sim 3.5\times10^{17}$ cm^{-3}) (see Supplementary Information); these will be referred to as p+, p, n+ and n henceforth. The silicon wafers were cleaned and deoxidised using H_2SO_4/H_2O_2 and HF based solutions in a controlled cleanroon environment (see Supplementary Information). Silicon wafers are ideal for the deposition of such thin films as their roughness is of the order of 1 nm. Aluminium Ohmic contacts were formed on the rear surface of the wafers to ensure a good electrical contact for the experiments (see Supplementary Information).

The contact angle data was gathered using a commercial Contact Angle Meter (GBX Scientific Instruments, France) (see Supplementary Information) and the experiments were performed in a class ISO 5/7 cleanroom (T = 20°C±0.5°C; RH = 45%±2%).

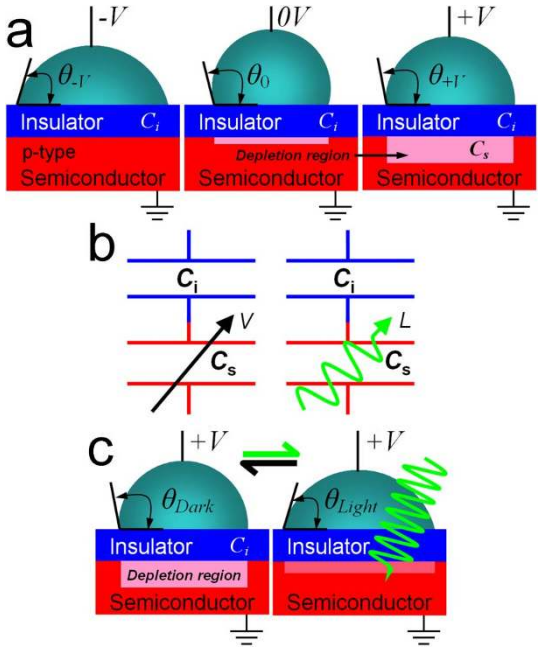

Figure 2 | Electrowetting and photoelectrowetting behaviour for the liquid-insulator-semiconductor system. a, The variation of the contact angle is not symmetrical with voltage polarity, $\theta_{-V} \neq \theta_{+V}$, due to the formation of a depletion region in the semiconductor under the insulator. The capacitance of the insulating layer is C_i Fm^{-2}; the voltage dependent capacitance of the semiconductor is C_s Fm^{-2}. b, Effect of illumination. Contact angle at positive bias (θ_{Dark}) for a p-type semiconductor and optically modified contact angle (θ_{Light}) at the same positive bias via the formation of photogenerated carriers (electron-hole pairs) in the semiconductor. The green arrow represents illumination using above band gap light. The arrows indicate that the effect is reversible. The photoelectrowetting angle modification $\Delta\theta_L = \theta_{dark} - \theta_{Light}$. c, Voltage and illumination dependent capacitances involved in electrowetting and photoelectrowetting.

Five liquids were used for the experiments: (i) a dilute hydrochloric acid solution (concentration = 0.01 M) (ii) two saline solutions (0.01 M and 0.001 M) (iii) an acetic acid solution (1 M) and Coca-Cola® (The Coca-Cola Company, USA). The electrical conductivities of the solutions were measured to be 3.64 mS cm^{-1}, 1.18 mS cm^{-1}, 0.12 mS cm^{-1}, 1.32 mS cm^{-1} and 1.07 mS cm^{-1} respectively (see Supplementary Information).

A small volume (~μL) of liquid was placed on the Teflon® surface. One contact was provided using the Ohmic contact on the rear surface of the wafers. The voltage (±40 V) was applied to the liquid via a stainless steel wire inserted into the droplet and the contact angle was recorded (photographed and filmed) (see Supplementary Information). The applied voltage was stepped to the measurement voltage V (see Supplementary Information).

Figure 3 shows photographs of the droplet profile as a function of applied voltage for the different silicon wafers under ambient room lighting (<10 W m^{-2}). For the two higher doped silicon wafers (p+ and n+) the contact angle measurements did not reveal a marked asymmetric contact angle variation with voltage polarity (Figure 3a and Figure 3b) behaving very much as the LIC system i.e. $\theta_{-V} \sim \theta_{+V}$. In contrast, in the case of the two lower doped silicon wafers (p and n) a distinct electrowetting asymmetry, depending on the voltage polarity, is observed (Figure 3c and Figure 3d). If we consider the p-type sample, a negative voltage leads to a contact angle variation similar to the p+ sample (Figure 3c). However, for a positive voltage the

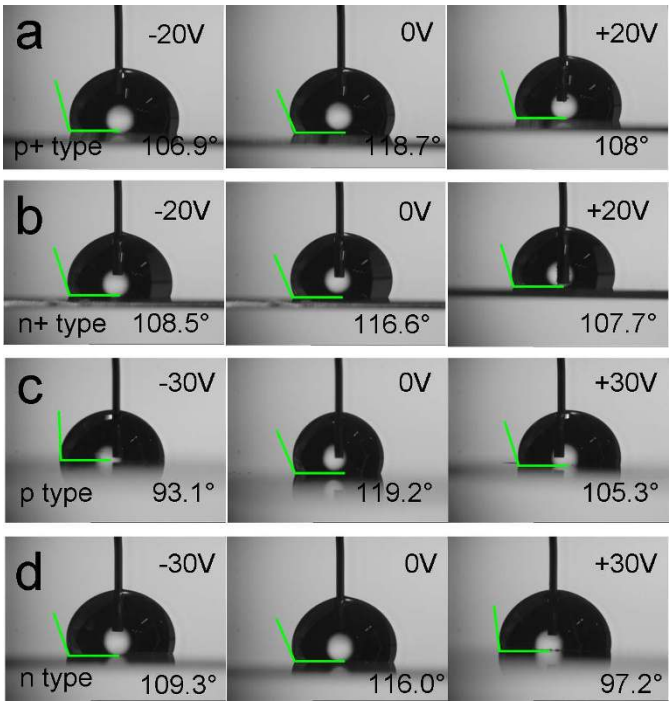

Figure 3 | Droplet profiles for electrowetting on Teflon® coated silicon wafers. a, p+ type. b, n+ type. c, p type and d, n type All silicon wafers were coated with a 265 nm thick layer of Teflon® AF. Liquid = HCl solution (0.01 M).

contact angle variation is less, i.e. the droplet tends not to spread out for positive applied voltages. The opposite is observed for the n-type silicon in terms of voltage polarity (Figure 3d), i.e. the droplet tends not to spread out for negative applied voltages.

Interestingly asymmetrical electrowetting[40] was reported for a silicon wafer (doping type and density not given in the paper) covered with a thin layer (100 nm) of Teflon® although this was attributed at the time to preferential adsorption of hydroxide ion, OH^- at Teflon® AF-water interfaces. The results here involving the highly doped silicon wafers (p+ and n+) point towards a semiconductor related effect, as is reported here, rather than a Teflon®-liquid interaction.

Figure 4 shows the effect of illumination on the droplet profile for the different silicon wafers and liquids. Under depletion conditions, i.e. a negative voltage for n-type and a positive voltage for p-type, illumination with an above band gap white light source (Schott, USA) (see Supplementary Information) leads to the expected flattening out of the droplet at constant voltage, i.e. the predicted photoelectrowetting effect. The photoelectrowetting effect is reversible, switching off the light source causes the droplet to "pop-up" and the dark contact angle is restored; the process can be repeated many times. As the voltage is increased on the droplet (positive for p-type, negative for n-type) the droplet flattens out more upon illumination, i.e. the illuminated contact angle (θ_{Light}) decreases with increasing voltage.

Figure 5 shows plots of the droplet contact angle as a function of applied voltage and illumination for the different silicon wafers. The two highly doped silicon wafers (p+ and n+) follow a classic relationship as expected from the Young-Lippmann equation (dashed black line) with C near constant. Figure 5 also shows the variation of droplet contact angle with illumination for the two lower doped silicon wafers (n and p). In contrast, the electrowetting for the lower doped p- and n-type silicon wafers does not at all follow a classic relationship for a positive and negative applied voltage respectively. In the case of the n-type wafer coated with 265 nm of Teflon® the

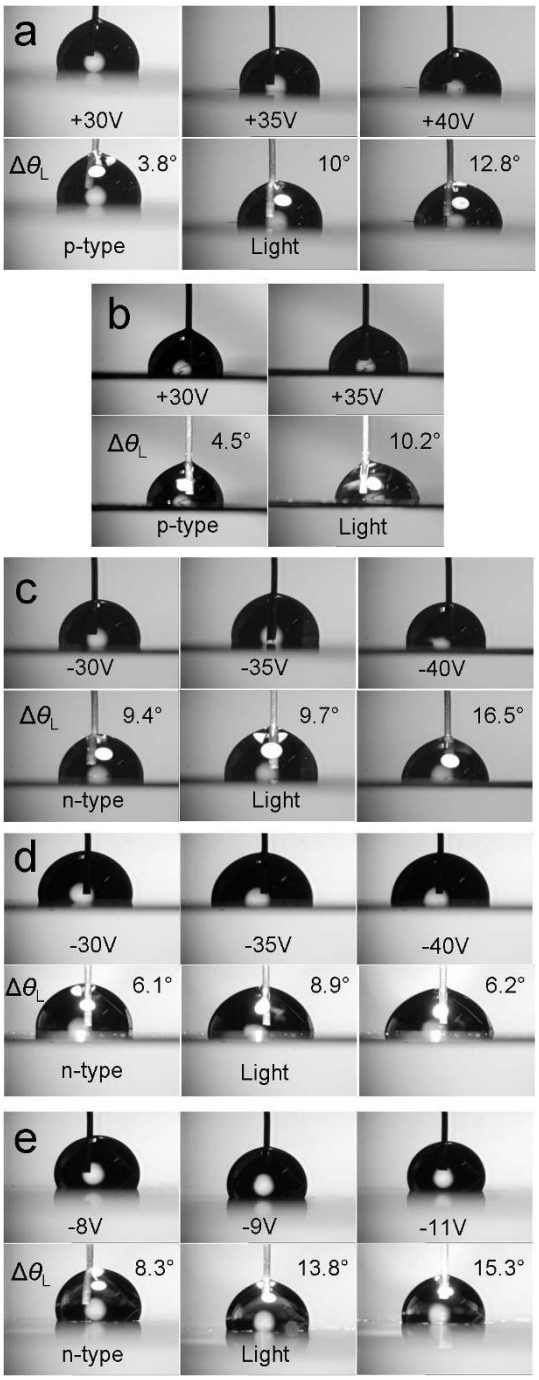

Figure 4 | The effect of illumination on droplets resting on Teflon® coated silicon wafers. a, p-type silicon coated with 265 nm of Teflon® using and HCl solution (0.01 M). b, p-type silicon coated with 265 nm of Teflon® using and Acetic acid solution (1 M). c, n-type silicon coated with 265 nm of Teflon® using and HCl solution (0.01 M). d, n-type silicon coated with 265 nm of Teflon® using Coca-Cola. e, n-type silicon coated with 20 nm of Teflon® using and NaCl solution (0.001 M). $\Delta\theta_L = \theta_{Dark} - \theta_{Light}$. Illumination was achieved using a white light source (Schott, USA).

contact angle at −30 V reduces by ~7° whereas at +30 V it reduces by ~20°. For the p-type wafer coated with 265 nm of Teflon®, the contact angle at −30 V reduces by ~26° whereas at +30 V it reduces by ~14°. The continuous coloured curves are based on results obtained during the electrical characterization (see later).

The largest optically induced contact angle change $\Delta\theta_L = \theta_{Dark} - \theta_{Light}$ equal to ~16° is observed for the n-type silicon at −40 V

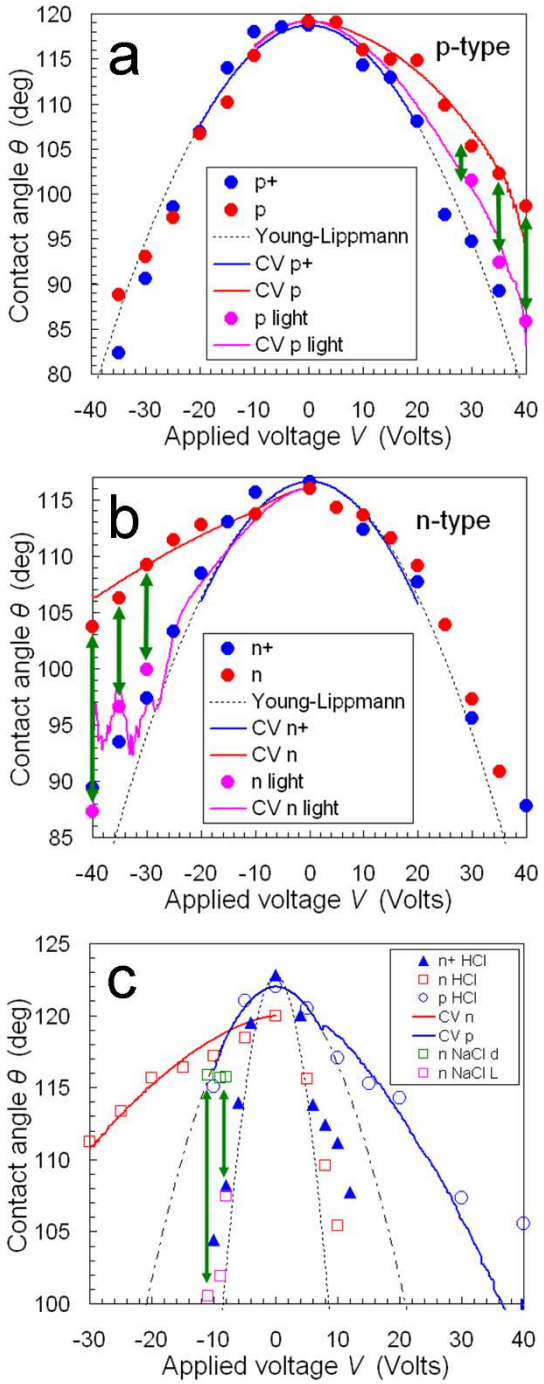

Figure 5 | Variation of droplet contact angle as a function of applied voltage and illumination for different silicon wafers coated with Teflon®. a, p+ (blue circles) and p-type silicon (red circles) coated with 265 nm of Teflon®. b, n+ (blue circles) and n-type silicon (red circles) coated with 265 nm of Teflon®. The contact angles under illumination are indicated by pink circles. c, n+ silicon (blue triangles) coated with 20 nm of Teflon® using an HCl (0.01 M) solution, n-type silicon (open red squares) coated with 20 nm of Teflon® using an HCl (0.01 M) solution, p-type silicon (open blue circles) coated with a 250 nm SiO_2 and 20 nm of Teflon® using an HCl (0.01 M) solution and n-type silicon (open green squares) coated with 20 nm of Teflon® using an NaCl (0.001 M) solution. The effect of illumination (open pink squares); the green arrows indicate reversibility. The dashed black lines correspond to the Young-Lippmann equation. The solid lines (red, blue and pink) correspond to the capacitance-voltage results (see later) injected into the Young-Lippmann equation. Room lighting measured to be <10 W m^{-2}. Illumination: p-type – 570 W m^{-2}, n-type - 1250 W m^{-2}.

(Figure 5b) although by reducing the thickness of the Teflon® from 265 nm to 20 nm on the n-type wafer a $\Delta\theta_L \sim 15^\circ$ can be achieved at voltages around 10 V (Figure 5c). The green arrows indicate reversibility.

The films (see Supplementary Information) enable a comparison of the time it takes the contact angle to adjust from θ_{Dark} to θ_{Light} and from θ_0 to $\theta_{\pm V}$ in the absence of illumination. These times were found to be comparable ($\sim$70 ms) supporting the view that the effect of light is to switch from a depleted state to an illuminated state[16,25] in the semiconductor via the generation of electron-hole pairs in the space-charge region. Additional experiments were preformed using bare silicon wafers not coated with Teflon® where a Schottky barrier is known to form[28,29]; a non-reversible photoelectrowetting effect was observed at low voltages (see Supplementary Information).

All this is well and good but in order to provide evidence that the photoelectrowetting and asymmetrical electrowetting effects observed here are related to *space-charge effects in the semiconductor* we need to look into what is happening *underneath* the surface. This can be done using impedance measurements.

Gold contacts (surface area $\sim$ 0.1–1 mm^2) were evaporated onto the Teflon®-silicon samples through a mechanical mask to form MIS structures. Impedance measurements were gathered using a Precision Impedance Analyzer (Agilent, USA) (see Supplementary Information).

Figure 6 shows the capacitance-voltage curves for the gold-Teflon®-silicon stacks. For the highest doped (p+) silicon wafer (black squares) the capacitance is constant [6.43×10^{-5} F m^{-2} ($\pm0.004\times10^{-5}$ F m^{-2})] over the voltage range ($\pm$20 V) (Figure 6a). The low frequency dielectric constant of the Teflon® can be extracted from this to be 1.92 ($\pm$0.04). For the next highest doped wafer (n+) (black circles), a slight carrier accumulation/depletion effect is observed with the capacitance varying from 6.26×10^{-5} F m^{-2} to 6.4×10^{-5} F m^{-2} as the voltage is increased from -20 V to $+20$ V (Figure 6a). Illumination using the white light source was observed to have little effect on the capacitance of these two samples just as illumination had no noticeable effect on the contact angle during the photoelectrowetting experiments for these samples (p+ and n+).

In terms of the lower doped samples (p and n), Figure 6b and Figure 6c show the variation of capacitance with voltage under background room lighting <10 W m^{-2} (black squares). In this case the capacitance is observed to vary strongly with voltage as the depletion width in the semiconductor is modified. The stacks behave similar to MIS system. For the n-type wafer coated with 265 nm of Teflon® the capacitance is reduced from 6.14×10^{-5} F m^{-2} to 1.2×10^{-5} F m^{-2} as the applied voltage is reduced from 0 V to -40 V. In the case of the p-type wafer coated with 265 nm of Teflon® the capacitance reduces to 3.1×10^{-5} F m^{-2} from 6×10^{-5} F m^{-2} as the voltage is increased from -10 V to $+40$ V.

Figure 6b and Figure 6c show the effect of illumination on the capacitance-voltage curves of the lower doped silicon wafers using above band gap light using the same white light source (Schott, USA) as used for the electrowetting experiments. As expected, the effect of illumination is to increase of the capacitance of the stacks[25]. It is this increase in capacitance that causes the droplet to spread out in the electrowetting experiments upon illumination. Indeed, the measured capacitance-voltage curves (dark and light) can now be inserted into the Young-Lippmann equation in order to compare the electrical characterization with the electrowetting characterization; these are the continuous coloured curves visible on Figure 5. The capacitance-voltage variations for the highly doped wafers (blue curves in Figure 5) follow the Young-Lippmann equation with C near constant. The capacitance-voltage variations for the lower doped wafers (red curves in Figure 5) do not follow the Young-Lippmann equation (with C constant) as C now varies with V. The capacitance variation observed during the impedance measurements under illumination fits very well with the contact angle variation upon illumination

during the photoelectrowetting experiments (pink curves in Figure 5). It is very clear that the electrical characterization gives very strong evidence that the asymmetrical electrowetting and photoelectrowetting observations here are semiconductor space-charge related effects[16].

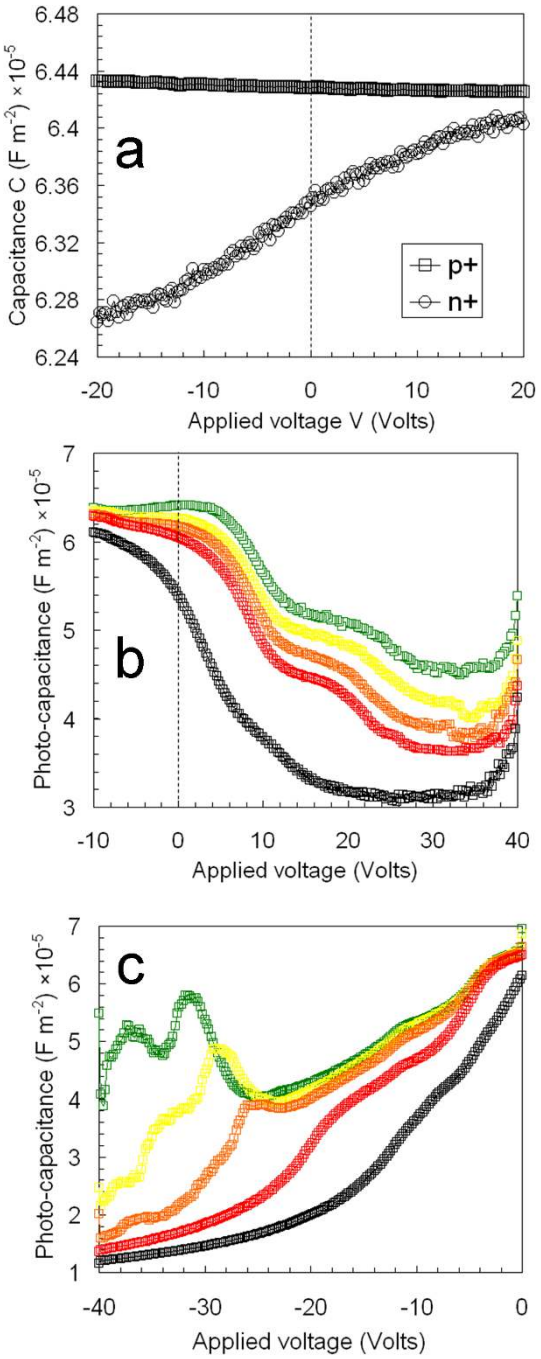

Figure 6 | Capacitance-voltage profiles of gold-Teflon®-silicon stacks. a, p+ and n+ silicon wafers coated with 265 nm of Teflon®. b, p-type silicon coated with 265 nm of Teflon®. c, n-type silicon coated with 265 nm of Teflon®. The coloured squares: red to green correspond to increasing light intensity. p-type: red = 350 W m^{-2}, orange = 500 W m^{-2}, yellow = 700 W m^{-2} and green = 1100 W m^{-2}. n-type: red = 200 W m^{-2}, orange = 1200 W m^{-2}, yellow = 2000 W m^{-2} and green = 2600 W m^{-2}. The black traces correspond to the measurement under room lighting <10 W m^{-2}. Measurement frequency for **a** = 10 kHz, **b** = 100 kHz, **c** = 10 kHz.

It was observed that the light intensity (or more correctly the *irradiance* W m^{-2}) required to vary the capacitance (during the impedance measurements) was greater than was necessary to produce the equivalent photoelectrowetting response by a factor of ~2–3. In order to understand why this is so the optical transmission into the silicon for the air-water-Teflon®-silicon and air-gold-Teflon®-silicon stacks was calculated (see Supplementary Information). The generation rate g cm^{-3} s^{-1} of photogenerated carriers in the silicon could thus be estimated and compared to an established photocapacitance model for MIS capacitors[25]. This calculation was in good agreement with observations and showed that (i) $g_{\text{photoelectrowetting}}/g_{\text{impedance}}$ ~3 for the same irradiance and (ii) $g_{\text{photoelectrowetting}} > 10^{20}$ cm^{-3} s^{-1} to produce the observed angle changes in the photoelectrowetting experiments. The photocapacitance model[25] yields a value of this order (see Supplementary Information). Going further, the MIS photocapacitance model[25] can be injected into the Young-Lippmann equation to calculate the variation of contact angle as a function of electron-hole pair generation rate g in the silicon (see Supplementary Information). The results of this are given in the following table and compare well with the experimental photoelectrowetting results given in Figure 4.

Discussion

In terms of optically induced liquid transport (thermal effects[11] aside), the literature is relatively scarce[41–46]. Laser-induced microflow due to vortices is possible[41,42] and an optically activated electrowetting has been reported[43]. However, this was due to a photoconductor used as a *lumped circuit element* rather than an intrinsic space-charge layer related effect which can be associated with the capacitance in the Young-Lippmann equation as is reported here. A "photo wetting" effect has also been reported using liquid crystals[44] but the physical mechanism responsible for the observations is not yet clear. Droplet transport has been achieved using light-induced chemical modification of a surface[45,46].

Another important point is that whereas droplet transport via electrowetting-on-dielectric[23,24] (EWOD) relies on complex electronic circuitry to apply a voltage locally to achieve contact angle modification. Here, in principle, droplet transport using a photoelectrowetting-on-semiconductors (PWOS) effect would render this circuitry, along with the necessary microtechnology to achieve it, redundant. Thus decreasing the complexity and costs. Therefore, in principle, a laboratory-on-a-chip[4] using PWOS for droplet transport would imply that the only micropatterning necessary would be for surface functionalization[8].

We are now in a position to understand the electrowetting and photoelectrowetting on semiconductors in terms of energy bands. Figure 7 illustrates the role of the carriers in the semiconductor in electrowetting and photoelectrowetting on a semiconductor coated with an insulator. If we take the example of an underlying p-type semiconductor; for a negative applied voltage then *accumulation* of carriers (holes) can occur near the insulator/semiconductor interface (Figure 7a)[16]; in this case the electrowetting behaviour will behave as

Table | Measured and modelled contact angle variation under illumination. The measured values are for silicon coated with 265 nm of Teflon® using a 0.01 M HCl solution. The calculated values use the photocapacitance model[25] injected into the Young-Lippmann equation

Depletion Voltage	p-type *Measured*	*Model*[25]	n-type *Measured*	*Model*[25]
30	3.8°	6.5°	9.4°	9.2°
35	10°	8.7°	9.7°	12.3°
40	12.8°	11.4°	16.5°	16°

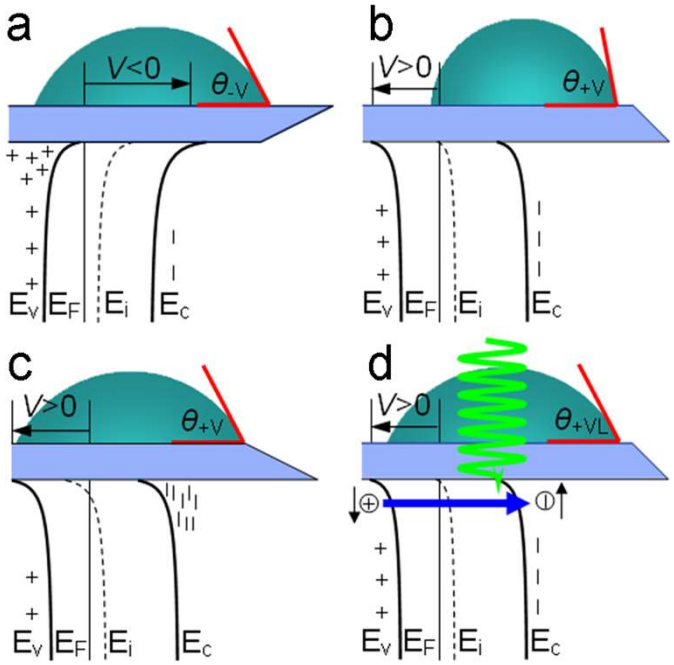

Figure 7 | The role of energy bands and carriers in electrowetting and photoelectrowetting for p-type silicon coated with an insulator. a, accumulation, b, depletion, c, inversion and d, illumination with above band-gap light under depletion. The insulator is light blue. The green arrow indicates illumination with above band-gap light; the blue arrow corresponds to electron-hole pair photogeneration. E_v, E_F, E_i and E_c correspond to the valence band energy, the Fermi energy, the intrinsic Fermi energy and the conduction band energy in the semiconductor.

the LIC system ($C = C_i$) and the droplet will spread out. If now we apply a positive voltage to the droplet, *depletion* of carriers (holes) will occur near the insulator/semiconductor interface and C_s will diminish with increasing voltage[16] resulting in less spreading out of the droplet (Figure 7b) as would occur at the equivalent negative voltage. If the positive bias is further increased then depending on doping level of the semiconductor carrier inversion (electrons) could occur[16] at the insulator/semiconductor interface leading to a re-emergence electrowetting as in the LIC system (Figure 7c). Under depletion, illumination using above band gap light generates electron-hole pairs in the space-charge region leading to an increase of the overall capacitance (Figure 7d) and spreading out of the droplet, i.e. photoelectrowetting.

As a last point, it is important to understand that the effects described here are *not* the result of simply adding a lumped element into the circuit[43] which acts as an optically controlled switch. On the contrary, the depletion layer in the underlying semiconductor is intrinsically responsible for the electrowetting and photoelectrowetting behaviour via the Young-Lippmann equation. Thus, the electrowetting and photoelectrowetting here is governed by the *bulk* electronic properties of the underlying semiconductor which allows the wetting to be controlled in a continuous way. The observations indicate a previously uncharted overlap between *capillary phenomena* and *semiconductor physics* which may prove to be valuable for the introduction of semiconductor effects into the above mentioned technologies[8–11] where wetting and capillary effects are fundamental.

Methods

Materials. The silicon wafers were purchased from Siltronix, France. Data concerning the silicon wafers can be found in the on-line Supplementary Information. The Teflon® AF 1600 was purchased from DuPont™, USA. The processing details of the Teflon® films can be found in the on-line Supplementary Information.

Experiments. Detailed information concerning all the photoelectrowetting, impedance and atomic force microscopy measurements can be found in the on-line Supplementary Information.

Additional experiments. All additional experiments and information on the movies taken during the experiments can be found in the on-line Supplementary Information.

1. Stone, H. A., Stroock, A. D. & Ajdari, A. Engineering flows in small devices. *Ann. Rev. Fluid Mech.*, **36**, 381–411 (2004).
2. Whitesides, G. M. The origins and the future of microfluidics. *Nature* **442**, 368–373 (2006).
3. Psaltis, D., Quake, S. R. & Yang, C. Developing optofluidic technology through the fusion of microfluidics and optics. *Nature* **442**, 381–386 (2006).
4. Craighead, H. Future lab-on-a-chip technologies for interrogating individual molecules. *Nature* **442**, 387–393 (2006).
5. Monat, C., Domachuk, P. & Eggleton, B. J. Integrated optofluidics: A new river of light. *Nature Photonics*, **1**, 106–114 (2007).
6. Mark, D., Haeberle, S., Roth, G., von Stetten, F. & Zengerle, R. Microfluidic lab-on-a-chip platforms: requirements, characteristics and applications. *Chem. Soc. Rev.*, **39**, 1153–1182 (2010).
7. Arora, A., Simone, G., Salieb-Beugelaar, G. B., Kim, J. T. & Manz, A. Latest Developments in Micro Total Analysis Systems. *Anal. Chem.*, **82**, 4830–4847 (2010).
8. Ghallab, Y. H. & Badawy, W. *Lab on a chip Techniques, Circuits and Biomedical Applications*. (Artech House USA, 2010).
9. Ducrée, J. J. & Zengerle, R. *Microfluidics (Microtechnology and MEMS)* (Springer USA, 2011).
10. Fainman, Y., Lee, L., Psaltis, D., & Yang, C. *Optofluidics: fundamentals, devices, and applications* (McGraw Hill USA, 2009).
11. Iverson, B. D. & Garimella, S. V. Recent advances in microscale pumping technologies: a review and evaluation. *Microfluid. Nanofluid.* **5**, 145–174 (2008).
12. Mugele, F. & Baret, J.-C. *Electrowetting: from basics to applications. J. Phys. Condensed Matter.* **17**, R705–R774 (2005).
13. Wheeler, A. R. Putting Electrowetting to Work. *Science* **322**, 539–540 (2008).
14. Abdelgawad, M. & Wheeler, A. R. The Digital Revolution: A New Paradigm for Microfluidics. *Adv. Mater.* **21**, 920–925 (2009).
15. Mugele, F. Fundamental challenges in electrowetting: from equilibrium shapes to contact angle saturation and drop dynamics. *Soft Matter* **5**, 3377–3384 (2009).
16. Sze, S. M. *Physics of semiconductor devices* 3rd Edition (Wiley, 2007).
17. de Gennes, P. G., Brochard-Wyart, F. & Quéré, D. *Capillarity and Wetting Phenomena* (Springer, 2004).
18. Lippmann G. Relations entre les phénomènes électriques et capillaires. *Ann. Chim. Phys.* **5**, 494 (1875).
19. Beni, G. & Hackwood, S. Electro-wetting displays. *Appl. Phys. Lett.* **38**, 207–209 (1981).
20. Hayes, R. A. & Feenstra, B. J. Video-speed electronic paper based on electrowetting. *Nature* **425**, 383–385 (2003).
21. Lee, J. & Kim, C.-J. Surface-Tension-Driven Microactuation Based on continuous electrowetting. *J. MEMS.* **9**, 171–180 (2000).
22. Berge, B. & Peseux, J. Variable focal lens controlled by an external voltage: An application of electrowetting. *Eur. Phys. J.* E **3**, 159–163 (2000).
23. Pollack, M. G., Fair, R. B. & Shenderov, A. D. Electrowetting-based actuation of liquid droplets for microfluidic applications. *Appl. Phys. Lett.* **77**, 1725–1726 (2000).
24. Cho, S. K., Moon, H. & Kim, C.-J. Creating, transporting, cutting, and merging liquid droplets by electrowetting-based actuation for digital microfluidic circuits. *IEEE J. Micromech. Sys.* **12**, 70–80 (2003).
25. Grosvalet, J. & Jund, C. Influence of illumination on MIS capacitance in the strong inversion region. *IEEE Trans. Electron Devices* **14**, 777–780 (1967).
26. Boyle, W. S. & Smith, G. E. Charge Coupled Semiconductor Devices. *Bell Sys. Tech. J.* **49**, 587–593 (1970).
27. Fossum, E. R. CMOS Image Sensors: Electronic Camera-On-A-Chip. IEEE Trans. *Electron. Dev.* **44**, 1689–1698 (1997).
28. Ambridge, T., Elliott, C. R. & Ambridge, T., Elliott, C. R. & Faktor, M. M. The electrochemical characterization of n-type gallium arsenide. *Journal of Applied Electrochemistry* **3**, 1–15 (1973).
29. Sharpe, C. D., Lilley, P., Elliott, C. R. & Ambridge, T. Electrochemical Carrier Concentration Profiling in Silicon. *Electronics Letters.* **15**, 622–624 (1979).
30. Blood, P. Capacitance-voltage profiling and the characterisation of III-V semiconductors using electrolyte barriers. *Semicond. Sci. Technol.* **1**, 7–27 (1986).
31. Bak, T., Nowotny, J., Rekas, M., Sorrell, C. C. Photo-electrochemical hydrogen generation from water using solar energy. Materials-related aspects. *International Journal of Hydrogen Energy* **27**, 991–1022 (2002).
32. Arutyunyan, V. M. Physical properties of the semiconductor-electrolyte interface. *Sov. Phys. Usp.* **3**, 521–542 (1989).
33. Fung, C. D., Cheung, P. W. & Fung, C. D., Cheung, P. W. & Ko, W. H. A Generalized Theory of an Electrolyte-Insulator-Semiconductor Field-Effect Transistor. *IEEE Trans. Electron Devices* **33**, 8–18 (1986).
34. Shinwari, M. W., Deen, M. J. & Landheer D. Study of the electrolyte-insulator-semiconductor field-effect transistor (EISFET) with applications in biosensor design. *Microelectronics Reliability* **47**, 2025–2057 (2007).

35. Prodromakis, T., Liu, Y., Constandinou, T., Georgiou, P. & C. Toumazou Exploiting CMOS Technology to Enhance the Performance of ISFET Sensors. *IEEE Electron Device Letters* **31**, 1053–1055 (2010).
36. Rosenblatt, S., Yaish, Y., Park, J., Gore, J., Sazonova, V. & McEuen, P. L. High Performance Electrolyte Gated Carbon Nanotube Transistors. *Nano Lett.* **2**, 869–872 (2002).
37. Verheijen, H. J. J. & Prins, M. W. J. Contact angle and wetting velocity measured electrically. *Rev. Sci. Instrum.* **70**, 3668–3673 (1999).
38. Uno, M., Tominari, Y., & Takeya, J. Fabrication of high-mobility organic single-crystal field-effect transistors with amorphous fluoropolymer gate insulators. *Organic Electronics* **9**, 753–756 (2008).
39. Shin, W. C., Shin, W. C., Seo, S., & Shin, W. C., Seo, S., & Cho, B. J. Highly air-stable electrical performance of graphene field effect transistors by interface engineering with amorphous fluoropolymer. *Appl. Phys. Lett.* **98**, 153505–3 (2011).
40. Moon, H., Moon, H., Cho, S. K., Moon, H., Cho, S. K., Garrell, R. L. & Kim C.-J. Low voltage electrowetting-on-dielectric. *J. Appl. Phys.* **92**, 4080–4087 (2002).
41. Nakano, M., Katsura, S., Touchard, G. G., Takashima, K. & Mizuno, A. Development of an optoelectrostatic micropump using a focused laser beam in a high-frequency electric field. *IEEE Trans. Ind. Appl.* **43**, 232–237 (2007).
42. Kumar, A., Williams, S. J. & Wereley, S. T. Experiments on opto-electrically generated microfluidic vortices. *Microfluidics and Nanofluidics*, **6**, 637–646 (2009).
43. Chiou, P. Y., Moon, H., Toshiyoshi, H., Kim, C. J., Wu, M. C. Light actuation of liquid by optoelectrowetting. *Sensors and Actuators* A **104** 222–228 (2003).
44. Goubert, G. & Galstian, T. Observation of a photo wetting effect on anisotropic liquid-solid interfaces. *Optics Express* **17**, 9637–47 (2009).
45. Ichimura, K., Oh, S.-K. & Ichimura, K., Oh, S.-K. & Nakagawa, M. Light-Driven Motion of Liquids on a Photoresponsive Surface. *Science* **288**, 1624–1626 (2000).
46. Berná, J., Leigh, D. A., Lubomska, M., Mendoza, S. M., Pérez, E. M., Rudolf, P., Teobaldi, G. & Zerbetto, F. Macroscopic transport by synthetic molecular machines. *Nature Mat.* **4**, 704–710 (2005).

Acknowledgements

The author would like to thank Gérard Cambien for technical help with the liquid resistivity measurements, Etienne Okada for technical help with impedance measurements and Dominique Deresmes for technical help with the AFM measurements.

Additional information

Supplementary information accompanies this paper at http://www.nature.com/scientificreports

Competing financial interests: The author declares no competing financial interests.

How to cite this article: Arscott, S. Moving liquids with light: Photoelectrowetting on semiconductors. *Sci. Rep.* **1**, 184; DOI:10.1038/srep00184 (2011).